

Investigation of Ground State Properties and Shape Evolution in Pt Isotopes

Y. El Bassem^{1,2}, M. Oulne¹

¹High Energy Physics and Astrophysics Laboratory, Department of Physics,
Faculty of Sciences SEMLALIA, Cadi Ayyad University,
P.O.B. 2390, Marrakesh, Morocco

²ERMAM, Polydisciplinary Faculty of Ouarzazate, Ibn Zohr University,
P.O.B 638, Ouarzazate, Morocco

Received 20 September 2021

Abstract. In this study, the ground-state properties of the platinum isotopic chain, $^{160-238}\text{Pt}$ are studied within the covariant density functional theory. The calculations are carried out for a large number of even-even Pt isotopes by using the density-dependent point-coupling and the density dependent meson-exchange effective interactions. Several ground-state properties such as the binding energy, separation energy and quadrupole deformation are discussed and compared with available experimental data, and with the predictions of some nuclear models such as the Relativistic Mean Field (RMF) model with NL3* functional and the Hartree Fock Bogoliubov (HFB) method with UNEDF0 Skyrme force. The shape phase transition for Pt isotopic chain is also studied.

KEY WORDS: Covariant density functional theory, ground-state properties, Pt isotopes, shape evolution.

1 Introduction

Density functional theories (DFT's) are extremely useful in understanding nuclear many-body dynamics. Among different nuclear DFTs, the covariant density functional theory (CDFT) [1–4] based on the energy density functionals (EDFs) is very successful in describing the ground and excited states throughout the chart of nuclei [5–7] as well as in the nuclear structure analysis [8–10]. In Ref. [11], the global performance of some covariant energy density functionals on some nuclear observables was analyzed.

In this work, we are interested in calculating and analyzing some ground-state properties of even-even Pt isotopes, $N = 82-160$, within the framework of

Table 1. Parameters of the DD-ME2 and DD-PC1 functionals

Parameter	DD-ME2	DD-PC1	Parameter	DD-ME2	DD-PC1
m	939	939	d_σ	0.4421	1.37235
m_σ	550.1238		a_ω	1.3892	5.91946
m_ω	783.000		b_ω	0.9240	8.86370
m_ρ	763.000		c_ω	1.4620	
g_σ	10.5396		d_ω	0.4775	0.65835
g_ω	13.0189		a_ρ	0.5647	
g_ρ	3.6836		b_ρ		1.83595
a_σ	1.3881	-10.04	d_ρ		0.64025 616
b_σ	1.0943	-9.150	δ_S		-0.8149 42
c_σ	1.7057	-6.42729			

the covariant density functional theory by using two functionals which provide a complete and an accurate description of different ground states and excited states over the whole nucleic chart [12–14], namely the density-dependent point-coupling DD-PC1 [15] and the density-dependent meson-exchange DD-ME2 [16], with the parameter sets listed in Table 1.

The paper is organized in the following way : The covariant density functional theory and details of the numerical calculations are presented in Section 2. Section 3 is devoted to the presentation of our results and the discussion. Finally, the conclusions of this study are presented in Section 4.

2 Theoretical Framework

Two classes of covariant density functional models are used throughout this paper: the density-dependent point-coupling (DD-PC) model and the density-dependent meson-exchange (DD-ME) model. The first has a finite interaction range and has been fitted to binding energies and radii of spherical nuclei; while the latter uses a zero-range interaction and has been fitted to nuclear matter data and for finite nuclei only to binding energies of a large range of deformed nuclei.

In the meson-exchange model, the nucleus is considered as a system of Dirac nucleons which interact via the exchange of mesons with finite masses leading to finite-range interactions [17, 18]. The standard Lagrangian density with medium dependence vertices that defines the meson-exchange model [19] is given by

$$\mathcal{L} = \bar{\psi}[\gamma(i\partial - g_\omega\omega - g_\rho\vec{\rho}\vec{\tau} - eA) - m - g_\sigma\sigma]\psi + \frac{1}{2}(\partial\sigma)^2 - \frac{1}{2}m_\sigma^2\sigma^2 - \frac{1}{4}\Omega_{\mu\nu}\Omega^{\mu\nu} + \frac{1}{2}m_\omega^2\omega^2 - \frac{1}{4}\vec{R}_{\mu\nu}\vec{R}^{\mu\nu} + \frac{1}{2}m_\rho^2\vec{\rho}^2 - \frac{1}{4}F_{\mu\nu}F^{\mu\nu}, \quad (1)$$

where m is the bare nucleon mass and ψ denotes the Dirac spinors. m_ρ , m_σ and m_ω are the masses of ρ meson, σ meson and ω meson, with the corresponding

coupling constants for the mesons to the nucleons as g_ρ , g_σ and g_ω respectively, and e is the charge of the proton.

The point-coupling model represents an alternative formulation of the self-consistent relativistic mean-field framework [20–23]. The Lagrangian for the DD-PC model [15, 24] is given by

$$\begin{aligned} \mathcal{L} = & \bar{\psi}(i\gamma \cdot \partial - m)\psi - \frac{1}{2}\alpha_S(\hat{\rho})(\bar{\psi}\psi)(\bar{\psi}\psi) - \frac{1}{2}\alpha_V(\hat{\rho})(\bar{\psi}\gamma^\mu\psi)(\bar{\psi}\gamma_\mu\psi) \\ & - \frac{1}{2}\alpha_{TV}(\hat{\rho})(\bar{\psi}\vec{\tau}\gamma^\mu\psi)(\bar{\psi}\vec{\tau}\gamma_\mu\psi) - \frac{1}{2}\delta_S(\partial_\nu\bar{\psi}\psi)(\partial^\nu\bar{\psi}\psi) \\ & - e\bar{\psi}\gamma \cdot A\frac{(1-\tau_3)}{2}\psi. \quad (2) \end{aligned}$$

The Eq. (2) contains the free-nucleon Lagrangian, the point coupling interaction terms, and the coupling of the proton to the electromagnetic field, the derivative terms account for the leading effects of finite-range interaction which are important in nuclei.

3 Results and Discussion

In this section, we present the ground-state properties of $^{160-238}\text{Pt}$ nuclei obtained in the framework of the CDFT by using the interactions DD-ME2 [16] and DD-PC1 [15]. Our results are compared with the available experimental data, the predictions of the RMF model with NL3* [18] functional and with the results of HFB theory with UNEDF0 [25] Skyrme force calculated by using the computer code HFBTHO v2.00d [26–29].

3.1 Binding energy

Binding energy (BE) is directly related to the stability of nuclei and is a very important quantity in nuclear physics. The total binding energies (BE) of ground states for platinum isotopes, $^{160-238}\text{Pt}$, are presented in Figure 1 as a function of the neutron number N . The available experimental data [30] as well as the predictions of the RMF(NL3*) [18] and HFB(UNEDF0) [25] theories are also shown for comparison.

It can be clearly seen from Figure 1 that the theoretical predictions reproduce the experimental data accurately and, qualitatively, all curves show a similar behavior.

In order to provide a further check of the accuracy of our results, the differences between the experimental total BE for even-even platinum isotopes and the calculated results obtained in this work are presented in Figure 2 as a function of the neutron number N .

Investigation of Ground State Properties and Shape Evolution in Pt Isotopes

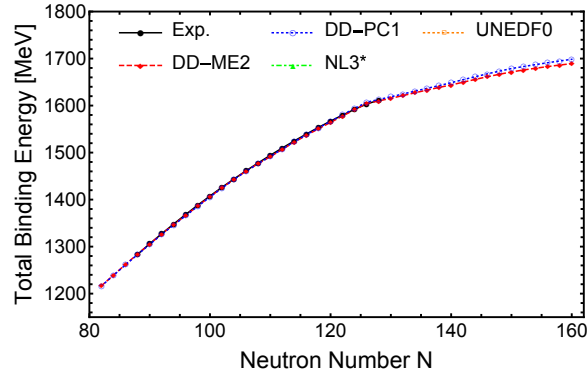


Figure 1. (Color online) The total binding energies for even-even $^{166-238}\text{Pt}$ isotopes.

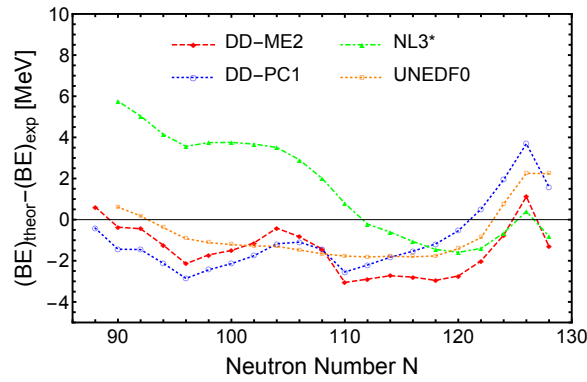


Figure 2. (Color online) Differences between theoretical total binding energies and experimental values for even-even Pt isotopes.

The comparison of the available experimental total binding energies of the ground state for $^{166-238}\text{Pt}$ with the present calculations and with the other theoretical models, is also done by the root mean square (rms) deviation tabulated in Table 2.

As we can see from Figure 2 and Table 2, UNEDF0 is more accurate than the other functionals DD-PC1, DD-ME2 and NL3*.

Table 2. The rms deviations of the total binding energies of platinum isotopes

DD-ME2	DD-PC1	NL3*	UNEDF0
1.864	1.880	2.8709	1.4454

3.2 Two neutron separation energy (S_{2n})

In the present work, we have calculated two-neutron separation energies, $S_{2n}(N, Z) = BE(N, Z) - BE(N - 2, Z)$, for Pt isotopes by using the density-dependent effective interactions DD-PC1 and DD-ME2.

In Figure 3, we display the calculated S_{2n} of even-even platinum isotopes, as a function of the neutron number N , in comparison with the available experimental data [30] and the predictions of RMF(NL3*) [18] and HFB(UNEDF0) [25].

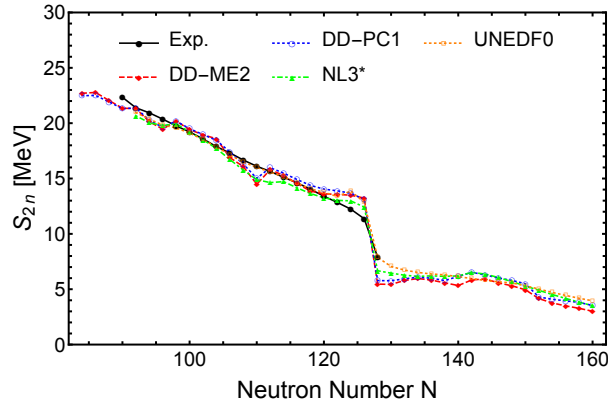


Figure 3. (Color online) The two-neutron separation energies, S_{2n} , for Pt isotopes.

As one can see from Figure 3, the results of the two density-dependent models DD-ME2 and DD-PC1 as well as those of NL3* and UNEDF0 reproduce the experimental data quite well except some small discrepancies which are mainly due to the missing beyond mean field corrections [31]. S_{2n} gradually decreases

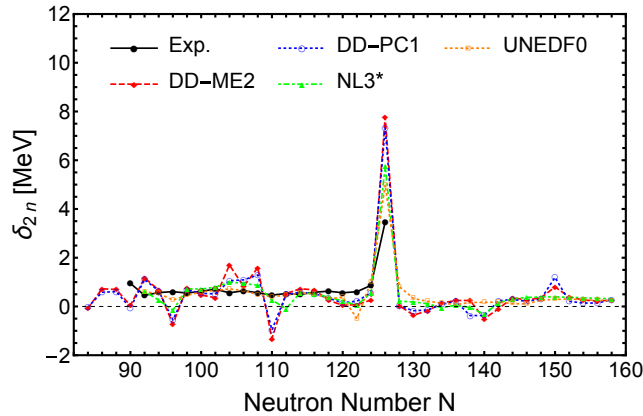


Figure 4. (Color online) δ_{2n} for even-even $^{94-168}\text{Pt}$ isotopes.

with N , and a sharp drop is distinctly seen at $N = 126$ in both experimental and theoretical curves, which corresponds to the closed shell at this magic neutron number.

A more sensitive observable for locating the shell closure is $\delta_{2n} = S_{2n}(N, Z) - S_{2n}(N + 2, Z)$. Figure 4 shows δ_{2n} as a function of the neutron number N . The strong peaking in (δ_{2n}) clearly seen at $N = 126$ further supports the shell closure at this neutron magic number as shown in Figure 3 by two-neutron separation energy (S_{2n}).

3.3 Quadrupole deformation

The quadrupole deformation is also an important property for describing the structure and shape of the nucleus. The quadrupole deformation parameter, β_2 , for Pt isotopes are plotted in Figure 5. Our results obtained with DD-ME2 and DD-PC1 parameter sets are compared with the available experimental data [32] and with the predictions of the RMF(NL3*) [18] and HFB(UNEDF0) [25] theories.

From Figure 5, one can see that the agreement between different theoretical calculations is pretty good in general.

All theoretical calculations predict spherical shapes around the neutron magic number $N = 126$. Nuclei with $84 \leq N \leq 90$ are predicted to be oblate in all theoretical calculations. The same is true for nuclei with $110 \leq N \leq 124$. The functionals DD-ME2, DD-PC and NL3* as well as the available experimental data predict the prolate shape in the regions $92 \leq N \leq 108$ and $N \geq 130$, while UNEDF0 shows an oblate shape for $94 \leq N \leq 108$ and $N \geq 146$.

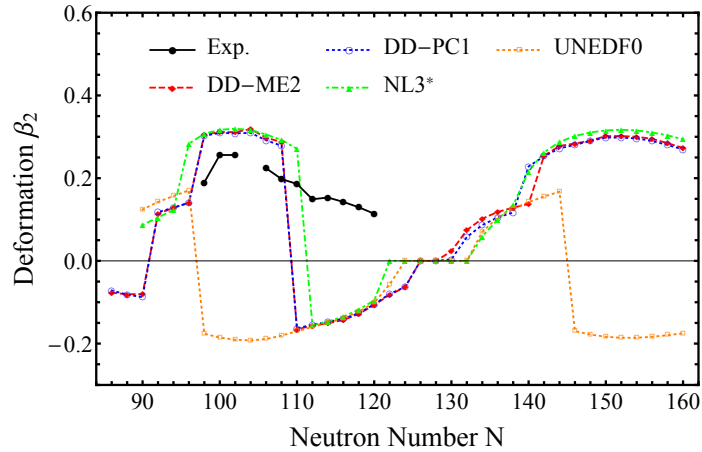


Figure 5. (Color online) The quadrupole deformation parameters, β_2 , for Pt isotopes.

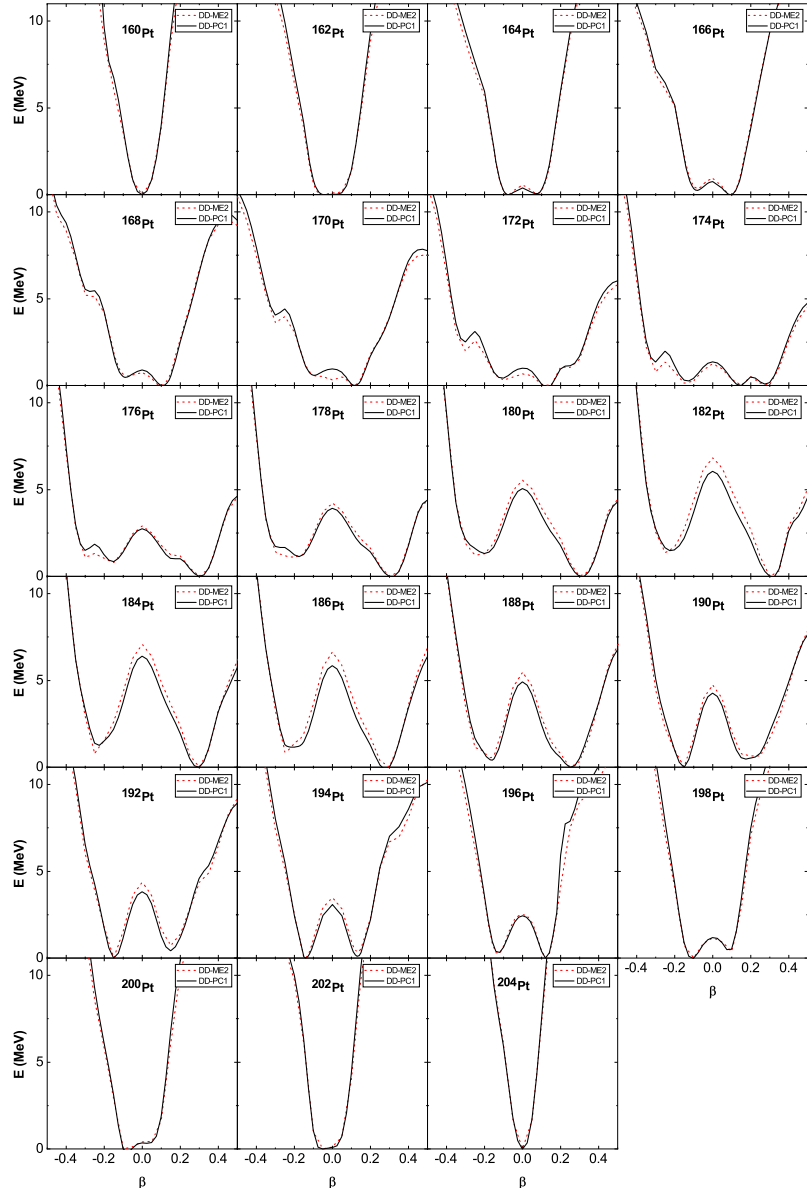


Figure 6. (Color online) The total energy curves for $^{160-204}\text{Pt}$ as a function of the axial quadrupole deformation parameter β_2 .

In Figure 6, we show for every Pt isotope (covering the mass interval $160 \leq A \leq 204$) the energy curves along the axial symmetry axis, as a function of

the deformation parameter, β , obtained within CDFT framework by using the density-dependent effective interactions DD-ME2 and DD-PC1.

As we can see from Figure 6, the interaction DD-PC1 provides potential energy curves which are extremely similar to the ones obtained with DD-ME2. The deformations of the oblate and prolate minima are practically independent of the force.

The lightest isotopes, $^{160-162}\text{Pt}$, exhibit spherical shape. The next isotope, ^{164}Pt , starts to develop two shallow degenerate minima, oblate and prolate, that correspond to a small value of β . The next isotope, ^{166}Pt , starts to develop a more pronounced prolate minimum. The $^{168-186}\text{Pt}$ isotopes show a similar structure, with a well-deformed prolate minimum, $\beta \approx 0.3$, and an oblate local minimum.

A transition from prolate to oblate shapes occurs smoothly between ^{188}Pt (prolate) and ^{190}Pt (oblate). In $^{190-200}\text{Pt}$ two minima appear, with the opposite situation occurring in $^{168-186}\text{Pt}$. As the mass number increases, the two well-deformed minima gradually disappear and we get a flat potential energy curve at $A = 202$. At $A = 204$, we get a sharp single minimum, which confirms the spherical shape at the magic neutron number $N = 126$.

These results are in good agreement with recent works [33–35]. However, other calculations have different results that are not in agreement with ours such as Ref. [36] which predicts that the shape transition in Pt isotopes within a beyond-mean-field approach with the Skyrme SLy6 occurs at $A = 186$ to 188 instead of $A = 188$ to 190 in our calculations. In the same line, constrained Hartree-Fock+ BCS calculations with the Skyrme forces Sk3, SGII, and SLy4 suggest a prolate to oblate shape transition at ^{182}Pt [37]. Furthermore, triaxial DIM-Gogny calculations predict a smooth shape transition at $A = 184$ to 186 [38].

These differences between theoretical methods in predicting the exact location of the shape transition are due, firstly, to the difference between the models used and, secondly, to the fact that the shape transition is very sensitive to the small details of the calculation because the shape transition occurs precisely around the region where the energies of the competing shapes are practically degenerate.

In Figure 7 we display the triaxial contour plots of $^{186-190}\text{Pt}$ isotopes in the (β, γ) plane. To study the dependency on γ , constrained triaxial calculations were made to map the quadrupole deformation space defined by β_2 and γ using the effective interaction DD-ME2.

The constrained calculations are performed by imposing constraints on both axial and triaxial mass quadrupole moments. The potential energy surface (PES) study as a function of the quadrupole deformation parameter is performed by the method of quadratic constraint [39] (see Ref. [40] for more details). Energies are normalized with respect to the binding energy of the global minimum such that the ground state has a zero MeV energy.

From this figure, we can notice that the location of the ground state minimum

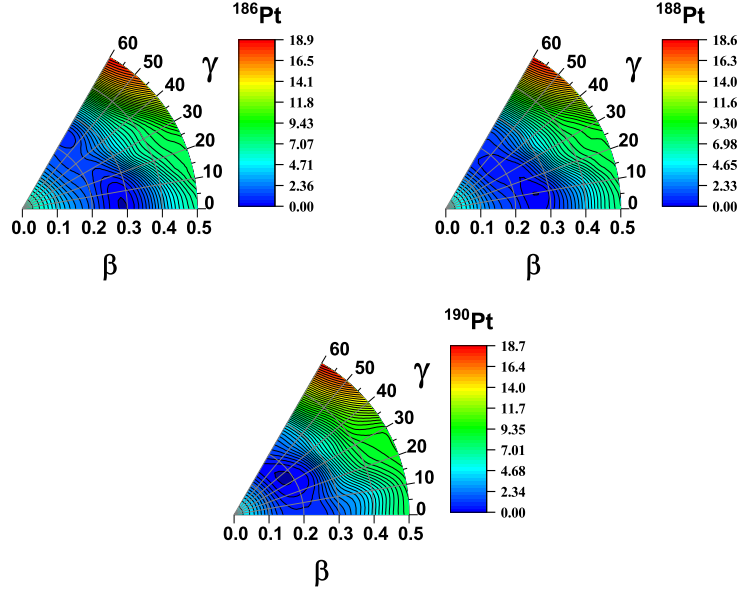


Figure 7. (Color online) Potential energy surfaces for $^{186-190}\text{Pt}$ in the (β, γ) plane, obtained from a CDFT calculations with the DD-ME2 parameter set. The color scale shown at the right has the unit of MeV, and scaled such that the ground state has a zero MeV energy.

moves from near prolate shape at ^{186}Pt to near oblate shape at ^{190}Pt . ^{188}Pt is slightly triaxial with its global minimum at $(0.25, 10^\circ)$. Thus, the shape transition is smooth, and there are no sudden changes in the nuclear shape. These results confirm those seen previously in Figure 6 and are in full agreement with the results shown in Figure 5 of Ref. [34] obtained with Hartree-Fock-Bogoliubov based on Gogny-D1S interaction.

4 Conclusion

In the present work, we have studied the ground state properties of even-even platinum isotopes, $^{160-238}\text{Pt}$, from the proton-rich side up to the neutron-rich one within the framework of the covariant density functional theory, by using two of the most recent functionals: The density-dependent point-coupling DD-PC1 and the density-dependent meson-exchange DD-ME2. The bulk ground state properties are quite well reproduced in our calculations and are in good agreement with the experimental data. A strong shell closure is clearly seen at $N = 126$. The total energy curves for $^{160-204}\text{Pt}$ obtained in this work suggest a smooth prolate to oblate shape transition at ^{188}Pt .

References

- [1] T. Nikšić, N. Paar, D. Vretenar, P. Ring (2014) *Comp. Phys. Commun.* **185** 1808.
- [2] G.A. Lalazissis, T. Nikšić, D. Vretenar, P. Ring (2005) *Phys. Rev. C* **71** 024312.
- [3] X. Roca-Maza, X. Viñas, M. Centelles, P. Ring, P. Schuck (2011) *Phys. Rev. C* **84** 054309.
- [4] T. Nikšić, D. Vretenar, P. Finelli, P. Ring (2002) *Phys. Rev. C* **66** 024306.
- [5] H. Abusara, A.V. Afanasjev, P. Ring (2012) *Phys. Rev. C* **85** 024314.
- [6] S.E. Agbemava, A.V. Afanasjev, T. Nakatsukasa, P. Ring (2015) *Phys. Rev. C* **92** 054310.
- [7] S.E. Agbemava, A.V. Afanasjev, D. Ray, P. Ring (2017) *Phys. Rev. C* **95** 054324.
- [8] J. Meng, S.G. Zhou (2015) *J. Phys. G* **42** 093101.
- [9] M. Matev, A.V. Afanasjev, J. Dobaczewski, G.A. Lalazissis, W. Nazarewicz (2007) *Phys. Rev. C* **76** 034304.
- [10] A.V. Afanasjev (2008) *Phys. Rev. C* **78** 054303.
- [11] S.E. Agbemava, A.V. Afanasjev, D. Ray, P. Ring (2014) *Phys. Rev. C* **89** 054320.
- [12] A. Karim, S. Ahmad (2015) *Phys. Rev. C* **92** 064608.
- [13] A.V. Afanasjev, H. Abusara (2010) *Phys. Rev. C* **81** 014309.
- [14] Y. El Bassem, M. Oulne (2019) *Nucl. Phys. A* **987** 16.
- [15] T. Nikšić, D. Vretenar, P. Ring (2008) *Phys. Rev. C* **78** 034318.
- [16] G.A. Lalazissis, T. Nikšić, D. Vretenar, P. Ring (2005) *Phys. Rev. C* **71** 024312.
- [17] S. Typel, H.H. Wolter (1999) *Nucl. Phys. A* **656** 331.
- [18] G.A. Lalazissis, S. Karatzikos, R. Fossion, D. Pena Arteaga, A.V. Afanasjev, P. Ring (2009) *Phys. Lett. B* **671** 36.
- [19] Y.K. Gambhir, P. Ring, A. Thimet (1990) *Ann. Phys. (NY)* **198** 132.
- [20] P. Manakos, T. Mannel (1988) *Z. Phys. A-Atomic Nuclei* **330** 223.
- [21] J.J. Rusnak, R.J. Furnstahl (1997) *Nucl. Phys. A* **627** 495.
- [22] T. Bürvenich, D.G. Madland, J.A. Maruhn, P.G. Reinhard (2002) *Phys. Rev. C* **65** 044308.
- [23] P.W. Zhao, Z.P. Li, J.M. Yao, J. Meng (2010) *Phys. Rev. C* **82** 054319.
- [24] B.A. Nikolaus, T. Hoch, D.G. Madland (1992) *Phys. Rev. C* **46** 1757.
- [25] M. Kortelainen, T. Lesinski, J. Moré, W. Nazarewicz, J. Sarich, N. Schunck, M.V. Stoitsov, S. Wild (2010) *Phys. Rev. C* **82** 024313.
- [26] M.V. Stoitsov, N. Schunck, M. Kortelainen, N. Michel, H. Nam, E. Olsen, S. Wild (2013) *Comput. Phys. Commun.* **184** 1592.
- [27] Y. El Bassem, M. Oulne (2015) *Int. J. Mod. Phys. E* **24** 1550073.
- [28] Y. El Bassem, M. Oulne (2017) *Nucl. Phys. A* **957** 22.
- [29] Y. El Bassem, M. Oulne (2017) *Int. J. Mod. Phys. E* **26** 1750084.
- [30] M. Wang, G. Audi, A.H. Wapstra, *et al.* (2012) The Ame2012 atomic mass evaluation. *Chin. Phys. C* **36** 1603.
- [31] E. Litvinova, P. Ring (2006) *Phys. Rev. C* **73** 044328.

- [32] S. Raman, C.W. Nestor Jr, P. Tikkanen (2001) *Atomic Data and Nuclear Data Tables* **78** 1-128.
- [33] R. Rodriguez-Guzman, *et al.* (2010) *Phys. Rev. C* **81** 024310.
- [34] J.E. Garcia-Ramos, *et al* (2014) *Phys. Rev. C* **89** 034313.
- [35] K. Nomura, *et al.* (2011) *Phys. Rev. C* **83** 014309.
- [36] J.M. Yao, M. Bender, P-H. Heenen (2013) *Phys. Rev. C* **87** 034322.
- [37] J.M. Boillos, P. Sarriguren (2015) *Phys. Rev. C* **91** 034311.
- [38] K. Nomura, R. Rodriguez-Guzman, L.M. Robledo (2013) *Phys. Rev. C* **87** 064313.
- [39] P. Ring, P. Schuck (1980) The Nuclear Many-Body Problem. *Physics Today* **103**(7) 70. DOI: [10.1063/1.2915762](https://doi.org/10.1063/1.2915762).
- [40] Z.P. Li, T. Nikšić, D. Vretenar, J. Meng, G.A. Lalazissis, P. Ring (2009) *Phys. Rev. C* **79** 054301.